

BIOCHEMISTRY

Computational design of a sensitive, selective phase-changing sensor protein for the VX nerve agent

James J. McCann^{1†}, Douglas H. Pike^{2†}, Mia C. Brown¹, David T. Crouse³, Vikas Nanda^{2*}, Ronald L. Koder^{1,4*}

The VX nerve agent is one of the deadliest chemical warfare agents. Specific, sensitive, real-time detection methods for this neurotoxin have not been reported. The creation of proteins that use biological recognition to fulfill these requirements using directed evolution or library screening methods has been hampered because its toxicity makes laboratory experimentation extraordinarily expensive. A pair of VX-binding proteins were designed using a supercharged scaffold that couples a large-scale phase change from unstructured to folded upon ligand binding, enabling fully internal binding sites that present the maximum surface area possible for high affinity and specificity in target recognition. Binding site residues were chosen using a new distributed evolutionary algorithm implementation in protCAD. Both designs detect VX at parts per billion concentrations with high specificity. Computational design of fully buried molecular recognition sites, in combination with supercharged phase-changing chassis proteins, enables the ready development of a new generation of small-molecule biosensors.

INTRODUCTION

Nerve agents have been implicated in several major world events over the past decade (1–3). VX, or *O*-ethyl *S*-[2-(diisopropylamino)ethyl] methylphosphonothioate, is an organophosphonate chemical warfare agent that acts as an acetylcholinesterase inhibitor at motor neuron junctions. By preventing the degradation of the neurotransmitter acetylcholine, VX exposure leads to continual activation of acetylcholine receptors, causing muscle paralysis and eventual death via asphyxiation within minutes (4). Lethal doses of VX are as little as 30 µg/kg (for oral administration), 70 µg/kg (for inhalation), or 86 µg/kg (for skin contact) (5). Atropine, 2-pyridine aldoxime methyl chloride, and benzodiazepines can be used to treat the symptoms of VX exposure if treatment has begun early enough (6). VX is a liquid at room temperature with a low vapor pressure and is relatively stable, breaking down via spontaneous hydrolysis over several days (7).

The high toxicity of VX necessitates that researchers either use less toxic analogs, such as the organophosphate insecticides parathion and demeton-S or other simulant molecules (Fig. 1) (8), or perform experiments in a limited number of authorized government facilities as outlined in the International Chemical Weapons Convention (9). Current methods for the rapid field detection of VX include direct detection via vehicle-mounted gas chromatography–mass spectrometric analysis (10), ion mobility spectrometry (11), colorimetric and electrodic sensors that use chemical reactions with the methylphosphonothioate moiety (12–14), or hybrid enzymatic systems that use natural acetylcholinesterase enzymes as a recognition element (8, 13). Each of these methods has advantages, but with the exception of spectrometry, the principal problem is the lack of specificity

of acetylcholinesterase and chemical reagents, resulting in false positives from insecticides and other organophosphates. Protein-based biological recognition, with its steric and electrostatic complementarity, offers the best path to a high-specificity real-time sensor. However, the inherent danger and high regulatory overhead of VX experimentation make the standard library screening or directed evolution approaches unfeasible. For these reasons, we set out to computationally design a VX-binding protein.

There have been a number of recent advances in the design of small-molecule binding proteins (15–18). These design approaches have targeted binding sites to protein surfaces or at interdomain interfaces. We reasoned that the utilization of a fully internal binding site would present a larger surface area for biological recognition, greatly easing the design of a high-affinity, high-specificity binding

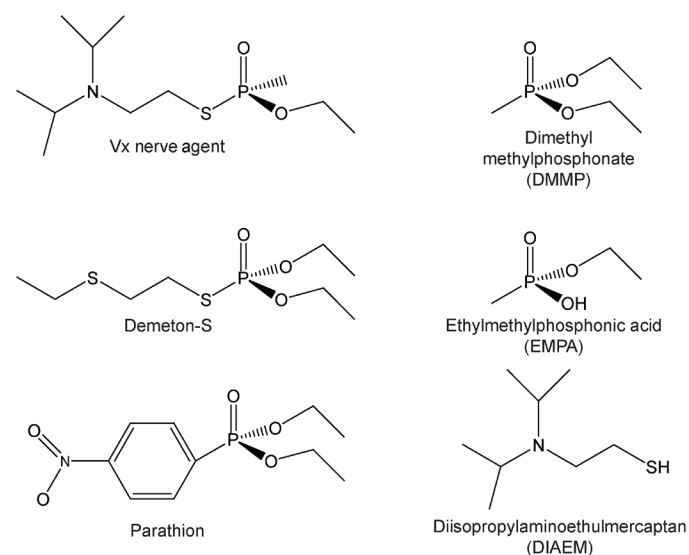


Fig. 1. The VX nerve agent, its simulant, and breakdown products. VX is chemically similar to both common organophosphates used as insecticides (left) (middle and bottom) and its still toxic breakdown products (right).

¹Department of Physics, The City College of New York, New York, NY 10031, USA.

²Center for Advanced Biotechnology and Medicine and the Department of Biochemistry and Molecular Biology, Robert Wood Johnson Medical School, Rutgers, The State University of New Jersey, Piscataway, NJ 08854, USA. ³Department of Electrical and Computer Engineering, Clarkson University, Potsdam, NY 13699, USA.

⁴Graduate Programs of Physics, Biology, Chemistry, and Biochemistry, The Graduate Center of CUNY, New York, NY 10016, USA.

*Corresponding author. Email: rkoder@ccny.cuny.edu (R.L.K.); vik.nanda@rutgers.edu (V.N.)

†These authors contributed equally to this work.

site. This necessitates the design of a protein that undergoes a large-scale conformational change concomitant with ligand binding. We recently reported a design algorithm for protein surface supercharging, in which a subset of fully surface-exposed side chains on proteins are changed to glutamate. Strong intrachain charge repulsion produces an unfolded protein, but structure can be restored by screening electrostatic forces at high ionic strengths. By poisoning the solution ionic strength, a phase transition from the unfolded apoprotein to a folded ligand-bound protein can be achieved (19). Using this approach, we introduced a VX-binding site into the core of a supercharged protein scaffold using a distributed evolutionary algorithm implemented in the protein design platform, protCAD (protein Computer Aided Design) (20).

RESULTS AND DISCUSSION

Developing a supercharged phase-changing scaffold protein for small-molecule binding

The designed four-helix bundle protein DRNN (21) was chosen as a chassis scaffold for small-molecule binding site insertion because it is well characterized structurally, it folds reversibly, it is extremely stable ($\Delta G_{\text{folding}} = -16.2$ kcal/mol), and helical bundles have been shown to have high designability compared to other folds (22). We then designed three variants of DRNN with net formal charge (the number of basic minus the number of acidic side chains), ranging from -17 to -37 (Fig. 2, A and B), and used circular dichroism (CD) to quantify their NaCl-dependent stability. Only the two most negatively charged variants were predominantly unfolded at low NaCl (Fig. 2, C and D), and we chose the more stable of the two, DRNN(-27), which is 50% folded at $\alpha_{\text{NaCl}} = 1.2$ M, as the optimal variant for binding site insertion.

VX-binding site design

The lowest-energy conformation of VX (23) was constructed using DrawMol (24), parameterized using AMBER tools antechamber, and

minimized with pmemd (table S1) (25). VX was aligned to the center of the four-helix bundle axis using protCAD. All positions that contacted or clashed with VX were sampled for design (Fig. 3, A and B). Random sequences were mapped on the experimental structure of DRNN (21) to generate a starting sequence pool. Next, a distributed evolutionary algorithm sampled these positions based on their frequency in top-scoring designs from prior generations (fig. S1). The simulation was stopped when the average enthalpy score of the sequence pool converged. Twenty top-scoring designs based on the computed score and chemical constraints were then selected for synthesis and characterization (Fig. 3C). All 20 designs had glycine residues at positions 22, 90, and 97, and positions 42 and 46 were glycine, serine, or alanine (fig. S2). These small amino acids provided room in the protein core to accommodate the neurotoxin, packing tightly against alkyl groups of VX.

VX protein selection, expression, and testing

The reaction between the VX nerve agent and human acetylcholinesterase involves the phosphorylation of an active site serine that is activated for nucleophilic attack as a consequence of its position at the terminus of a Glu-His-Ser catalytic triad (26). In supercharged DRNN, it is possible that a similar covalent modification, followed by the release of the bulk of the VX molecule, could result in the refolding of the protein and a concomitant loss of signal. However, absent activation by the catalytic triad serine is a poor nucleophile for organophosphates, while carboxylates such as acetate do catalyze organophosphate hydrolysis (27). The positive charge at the phosphorus in VX results in a high likelihood of negatively charged Glu and Asp counterions in the lowest-energy models. Such carboxylates can act as nucleophiles even in the absence of activation. For this reason, we selected the 10 lowest-energy designs that did not introduce carboxylate side chains into the binding site. We also chose the 10 lowest-energy designs that contain carboxylate ions at these positions (sequences and energies in table S2, and coordinates of all 20 models are in table S3). Genes were synthesized for the 20 final designs,

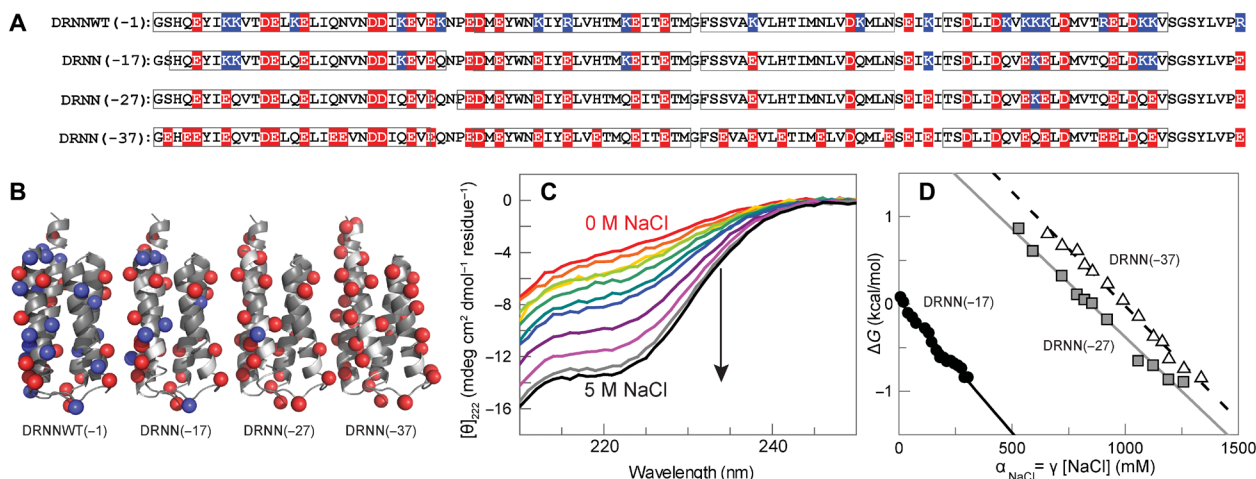


Fig. 2. Chassis design. (A) Sequences of DRNN and its derivatives. Net charge in parentheses. Basic (blue) and acidic (red) residues are highlighted. The four α -helical elements in each design are boxed. (B) Spatial distribution of acidic (red) and basic (blue) side chains. Spheres are the beta carbons of each ionizable residue. (C) NaCl-dependent CD-monitored folding of DRNN(-27) at pH 7.0. Limiting spectra at 0 M NaCl and 5 M NaCl in units of mean residue ellipticity are depicted in red and black, respectively. (D) Folding energy of supercharged DRNN derivatives as a function of NaCl activity.

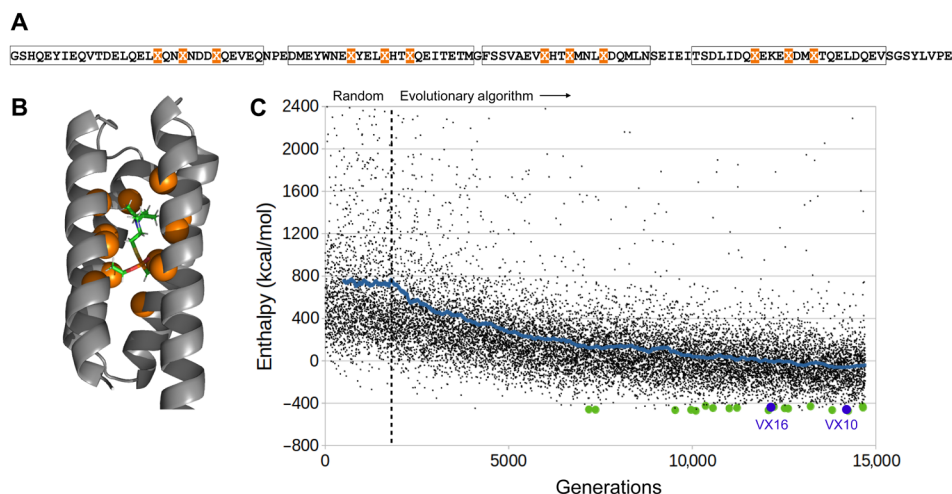


Fig. 3. VX-binding site design. (A) Core positions to be sampled during design are highlighted in orange, chosen on the basis of contact with a centrally placed VX molecule (16). (B) Orange spheres show sampled positions in the DRNN structure. (C) A distributed evolutionary algorithm protocol was used to sample core positions. An initial randomization phase was used to generate the sequence pool, followed by an annealing phase using top-scoring sequences from the pool. Each point is one final structure/sequence enthalpy score; the blue line is the average score per generation. Best scoring designs were selected for characterization (green dots). Two successful variants were found (blue dots).

VX1 to VX20, which combine core binding site substitutions with surface supercharging substitutions from DRNN(−27). These were expressed in *Escherichia coli* and purified.

In the absence of VX, all 20 proteins exhibited CD spectra indicative of random coil structure at high and low α_{NaCl} at pH 7.0. At pH 3.5, reduced charge repulsion from protonation of surface glutamates enabled a subset of designs to form helices at high α_{NaCl} (fig. S3), possibly a result of condensed molten globule formation in the absence of ligand (19).

As the Chemical Weapons Convention stipulates, experiments performed using VX must take place in specialized facilities, and any equipment used to perform these experiments must be incinerated after use (9). The high cost of CD spectrometers drove us to find another signifier of the protein folding state. DRNN(−27) has a buried tryptophan that is unchanged in all designs (Fig. 4B). This residue exhibits a substantial change in fluorescence intensity when the protein unfolds (fig. S4), making fluorescence a sensitive measure of concerted folding and binding. Quenching of tryptophan occurs at low pH (28) due to protonation of the indole group. Our molecular design places tryptophan in the protein core, shielding it from interactions with the low-pH environment in the folded state, consistent with the large intensity change upon unfolding. We constructed an inexpensive fluorescence spectrometer using a white light-emitting diode, a pair of low- and high-pass filters, and a detector photodiode at a 90° angle (fig. S5). This simple spectrometer is connected to a voltmeter via a wire to the outside of the testing hood, and tryptophan fluorescence can be safely quantified.

Using this device, we screened the response of all 20 proteins to two different concentrations of VX (fig. S6) at pH 3.5. Two of them, VX10 and VX16 (Fig. 4A), exhibited increases in fluorescence in response to moderate concentrations of VX that are proportional to the increase in fluorescence that they exhibit upon folding at high α_{NaCl} as detected by both CD and infrared spectroscopy (fig. S7 and table S4). We then examined the VX-binding affinity of each in more detail (Fig. 4D): At pH 3.5, VX10 binds VX with a dissociation constant of 700 ± 100 nM, and VX16 binds VX with a dissociation constant

of 330 ± 40 nM. These affinities correspond to mass concentrations of 190 ± 30 and 90 ± 10 parts per billion, respectively, each more than two orders of magnitude lower than the toxic concentration in humans (29). Both proteins display less than a 1% response to micromolar concentrations of the VX simulants parathion or demeton-S (Fig. 4E) or the toxic VX breakdown products DIAEM [2-(diisopropylamino) ethyl mercaptan], DMMP (dimethyl methylphosphonate), or EMPA (ethylmethylphosphonic acid) (Fig. 4F). Figure S8 enumerates computed residue-ligand interaction energetics and key interactions in VX10 and VX16 based on the two structural models.

At pH 7.0, the fluorescence of both proteins decreases upon folding, albeit to a smaller magnitude than the increase at pH 3.5 (fig. S9A). As expected, both proteins exhibit decreases in fluorescence upon VX binding at this pH (fig. S9B). VX16 binds VX with a dissociation constant of 380 ± 90 nM, while the low signal-to-noise ratio, given the relatively small decrease in fluorescence of VX10, allows us only to determine that the dissociation constant is less than 100 nM.

The large-scale phase changes imparted on the structure of DRNN by surface protein supercharging have enabled us to implant a VX-binding site into its center. Using this approach, in concert with a computational optimization of the internal binding site, we designed two different proteins that bind VX with dissociation constants that are more than two orders of magnitude lower than the concentrations identified as toxic by the Board on Environmental Studies and Toxicology (BEST) of the National Academies (29). As the actual detection limits are at least ninefold lower than these dissociation constants (Fig. 4D, inset) (30), both proteins detect VX in water at concentrations at least three orders of magnitude lower than toxicity. Furthermore, this sensor does not recognize simulants or breakdown products, is reagentless, and has a response time of seconds. These detection limits have been achieved without optimization of the surface supercharging—a larger folding energy penalty weakens binding (19)—and it seems likely that lowering the extent of the supercharging would both enhance the affinity of VX10 and VX16 for VX, decreasing detection limits even further, and enable some of the remaining binding site designs in the library to respond to VX.

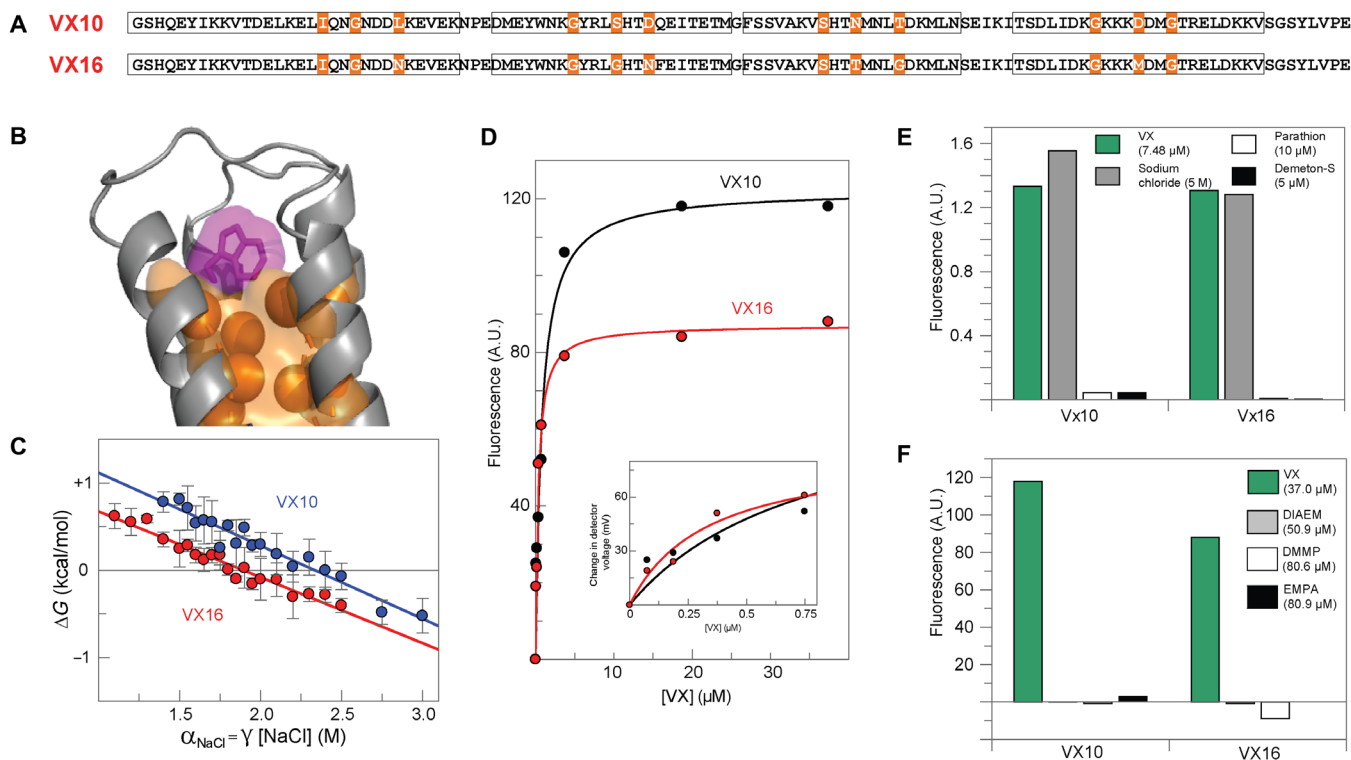


Fig. 4. Sensitivity and specificity of two designed VX-binding proteins. (A) Sequences of VX10 and VX16 with VX-interacting positions highlighted in orange. (B) The buried tryptophan shown in purple and the optimized binding site in orange. (C) NaCl-induced folding of apo-VX10 (blue) and apo-VX16 (red) at pH 3.5 detected using tryptophan fluorescence. (D) VX binding by VX10 (black) and VX16 (red). Lines drawn are fits with the single site binding equation with K_D values of 700 ± 100 and 330 ± 40 nM, respectively. Inset: Change in detector voltage at low VX concentrations showing the high sensitivity of this measurement. (E) The response of VX10 and VX16 to the organophosphate VX simulants parathion and demeton-S. (F) The response of VX10 and VX16 to known VX breakdown products. A.U., arbitrary units.

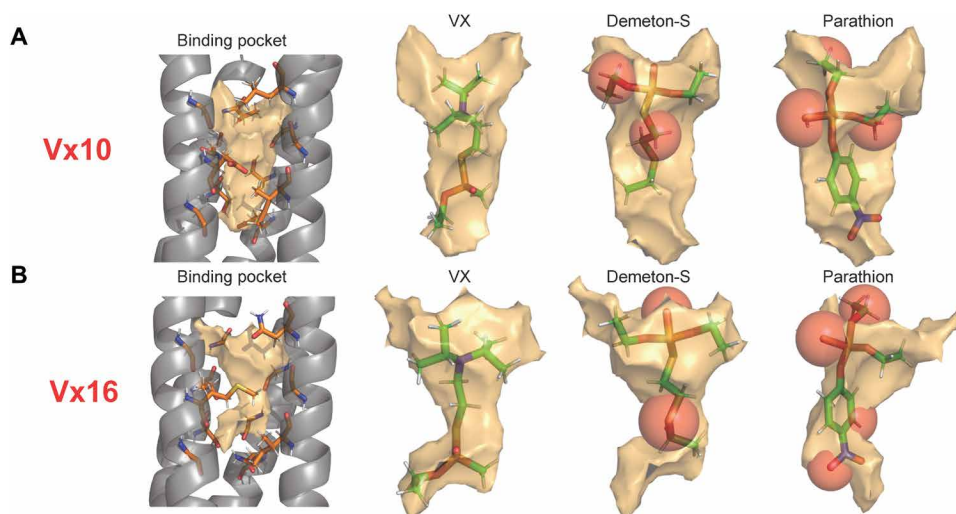


Fig. 5. Steric exclusion of the VX simulants demeton-S and parathion. The VX-binding cavities of (A) VX10 and (B) VX16 proteins are depicted in tan, and steric clashes from bound simulants are depicted as red spheres.

The fully internal binding site enables stabilizing interactions with the entire surface area of the ligand, and the form-fitting binding pocket imparts an implicit negative design—differently shaped VX simulants have significant steric clashes with the folded proteins (Fig. 5). VX breakdown fragments have less interaction surface area

and leave destabilizing cavities in the folded proteins, and therefore, binding is similarly inhibited.

The design method presented here should enable the development of a new generation of biosensors, therapeutics, and diagnostics. The combination of the phase-changing supercharged DRNN(-27)

chassis protein and computational design promises the ready development of sensitive, selective small-molecule sensors. While we describe a simple VX detector that can be built for less than \$5000, this protein and the others designed using this method can be incorporated as the recognition element in any number of protein biosensor platforms that can take advantage of the large-scale phase change engendered by supercharging, including surface plasmon resonance–based protein–ligand complex formation sensors (31) and protein folding–based electrochemical detection schemes (32), to greatly enhance sensitivity.

MATERIALS AND METHODS

Design of supercharged protein

Starting with the crystal structure of DRNN (Protein Data Bank ID: 3U3B), surface-exposed residues on the α helices were mutated to either alanine or glutamic acid. In the case of DRNN(–17), positively charged (lysine and arginine) residues were mutated to alanine, increasing the net negative charge of the protein. For DRNN(–27), these same residues were mutated to glutamic acid, further increasing the net negative charge. For DRNN37, additional surface-exposed sites were selected for the mutation of neutral amino acids to glutamic acid.

VX force field parameterization

The VX two-dimensional (2D) chemical structure was downloaded from ChemSpider (33) with ID: 36386. DrawMol was used to pre-optimize the 3D bond angles and torsions using the UFF (Universal force field) before force field parameterization in AMBER (34). Partial static charges were calculated for VX using the AM1-BCC method (35) in AMBER's antechamber software. VX van der Waals atom-type assignments and harmonic bond potentials were determined using antechamber for use with the GAFF (general AMBER force field) (36).

protCAD computational binding site design

protCAD is a computational design platform developed by Summa *et al.* (37) and currently maintained by Pike and Nanda (20). The program allows sampling of protein motions in torsional space and sequence substitutions. Scoring includes AMBER ff14SB (38) nonbonding terms, the Dunbrack bbdep rotamer library (39), and implicit solvation using a local dielectric term (20). The software library, manual, and example programs are available for download from github.com/protcad/protcad.

Design of the VX-binding sites in DRNN(–27) was performed using the program protEvolver, which can repack a protein fold with or without local backbone flexibility, using a distributed evolutionary algorithm that proceeds in two stages: a randomization stage where the initial sequence pool is created, and an exploration stage where sequences are optimized on the basis of amino acid frequencies in the pool. The program can be run on a single thread or distributed across multiple nodes. The protEvolver code can be found at <https://doi.org/10.5281/zenodo.6539666>.

VX was placed at the center of DRNN and aligned so that the long axis of the ligand coincided with the superhelical axis of the protein. Twelve positions, three for each helix of DRNN, were selected for repacking around VX. In the first stage of repacking by protEvolver, 2000 randomized initial sequence variants were constructed. Each variant was subject to repacking, allowing for all amino acids at equal probability at the 12 positions. Side-chain rotamer optimization was performed using all backbone-independent rotamers

followed by fine rotational sampling (1° increments) to optimize interactions with VX. Mutations were accepted if the energy change was less than kT ($T = 300$ K; 0.5 kcal/mol). Sequence optimization continued until a fixed number of consecutive failures—in this case, 15—has been reached. A total of 2000 initial sequences were generated, after which the best half were retained for the second stage of repacking. The remaining models were not used to bias sampling frequency of mutation.

In the second exploratory stage, a generation of new sequences was created by applying the same mutational scheme except that mutations were weighted on the basis of a probability equal to their position-specific frequency in the sequence pool. Amino acid types not present at a position in the pool were assigned a minute but nonzero probability, allowing for innovation. Mutations would continue to accumulate in a new model until 15 consecutive rejections have been reached. Final models from the current cycle were included in the sequence pool, and the best 1000 were retained, with the remainder discarded. This was continued with each generation by selecting amino acid probabilities based on the previous sequence pool. The calculation was terminated when the mean interaction score of the pool converged.

Purification of designed proteins

All DRNN and VX-binding proteins were expressed in HMS174 *E. coli* cells as a 6xHis-tagged thioredoxin fusion protein from the pET32a vector. Briefly, cells were grown at 37°C until they reached an optical density of 0.6, after which 0.5 mM isopropyl- β -D-thiogalactopyranoside was added, and the temperature was lowered to 18°C for overnight expression. Standard protocols (40) for the purification of 6-his-tagged proteins were followed, except that the sodium chloride concentration was raised to 1 M to prevent non-specific binding. Following Ni-NTA (nitrilotriacetic acid) purification and the cleavage of the thioredoxin tag with TEV protease, the supercharged proteins were further purified using a DEAE anion exchange column. Purified proteins were dialyzed into 50 mM sodium phosphate and 300 mM sodium chloride (pH 8) for storage and shipping.

Circular dichroism

CD measurements were made using an Aviv model 400 spectrometer at a protein concentration of 10 μM .

Intrinsic fluorescence

Fluorescence measurement to measure the salt-induced folding and off-target organophosphate binding was performed using an Olis DM45 spectrofluorimeter. Samples were excited at 280 nm while monitoring the fluorescence emission at 348 nm.

VX measurements

Measurements were performed at the approved chemical weapon testing facility at MRIGlobal (Kansas City, MO). For the VX-binding experiments, the intrinsic fluorescence was monitored using a simplified custom-built fluorimeter (see fig. S4). For the fluorescence measurements, the VX nerve agent and its breakdown products were diluted to 10 μM into either citrate buffer (50 mM sodium citrate and 1500 mM sodium chloride) or Hepes buffer [20 mM Hepes and 1000 mM sodium chloride (pH 7)]. In each experiment, proteins were purified at The City College of New York, concentrated using spin concentrators, shipped in ice overnight to MRIGlobal, and tested within 24 hours of purification.

SUPPLEMENTARY MATERIALS

Supplementary material for this article is available at <https://science.org/doi/10.1126/sciadv.abh3421>

[View/request a protocol for this paper from Bio-protocol.](#)

REFERENCES AND NOTES

- J. Brooks, T. B. Erickson, S. Kayden, R. Ruiz, S. Wilkinson, F. M. Burkle Jr., Responding to chemical weapons violations in Syria: Legal, health, and humanitarian recommendations. *Confl. Health* **12**, 12 (2018).
- R. C. Paddock, C. Sang-Hun, in *The New York Times* (The New York Times Inc., 2017).
- M. Schwartz, M. Eddy, in *The New York Times* (The New York Times Inc., 2020).
- C. H. Gunderson, C. R. Lehmann, F. R. Sidell, B. Jabbari, Nerve agents: A review. *Neurology* **42**, 946–950 (1992).
- M. Moshiri, E. Darchini-Maragheh, M. Balali-Mood, Advances in toxicology and medical treatment of chemical warfare nerve agents. *Daru* **20**, 81 (2012).
- D. T. Lawrence, M. A. Kirk, Chemical terrorism attacks: Update on antidotes. *Emerg. Med. Clin. N. Am.* **25**, 567–595 (2007).
- C. Schneider, A. Bierwisch, M. Koller, F. Worek, S. Kubik, Detoxification of VX and other V-type nerve agents in water at 37 °C and pH7.4 by substituted sulfonatocalix 4 arenes. *Angew. Chem. Int. Ed. Engl.* **55**, 12668–12672 (2016).
- A. Coban, R. L. Carr, H. W. Chambers, K. O. Willeford, J. E. Chambers, Comparison of inhibition kinetics of several organophosphates, including some nerve agent surrogates, using human erythrocyte and rat and mouse brain acetylcholinesterase. *Toxicol. Lett.* **248**, 39–45 (2016).
- O. Thraenert, The international chemical weapons convention—Problems involved. *Aussen Polit.* **44**, 222–231 (1993); <https://doi.org/10.1515/sirius-2020-3008>.
- Y. Ohrui, T. Nagoya, N. Kurimata, M. Sodeyama, Y. Seto, Identification of V-type nerve agents in vapor samples using a field-portable capillary gas chromatography/membrane-interfaced electron ionization quadrupole mass spectrometry instrument with Tri-Bed concentrator and fluoridating conversion tube. *J. Mass Spectrom.* **52**, 472–479 (2017).
- M. A. Makinen, O. A. Anttalainen, M. E. T. Sillanpaa, Ion mobility spectrometry and its applications in detection of chemical warfare agents. *Anal. Chem.* **82**, 9594–9600 (2010).
- M. C. de Koning, G. W. Peterson, M. van Grol, I. Iordanov, M. McEntee, Degradation and detection of the nerve agent VX by a chromophore-functionalized zirconium MOF. *Chem. Mater.* **31**, 7417–7424 (2019).
- M. Pohanka, J. Z. Karasova, K. Kuca, J. Pikula, O. Holas, J. Korabecny, J. Cabal, Colorimetric dipstick for assay of organophosphate pesticides and nerve agents represented by paraoxon, sarin and VX. *Talanta* **81**, 621–624 (2010).
- M. Pohanka, M. Hrabivova, K. Kuca, Diagnosis of intoxication by the organophosphate vx: Comparison between an electrochemical sensor and Ellman's photometric method. *Sensors* **8**, 5229–5237 (2008).
- N. F. Polizzi, W. F. DeGrado, A defined structural unit enables de novo design of small-molecule-binding proteins. *Science* **369**, 1227–1233 (2020).
- M. J. Bick, P. J. Greisen, K. J. Morey, M. S. Antunes, D. Ia, B. Sankaran, L. Raymond, K. Johnsson, J. I. Medford, D. Baker, Computational design of environmental sensors for the potent opioid fentanyl. *eLife* **6**, e28909 (2017).
- A. Quijano-Rubio, H. W. Yeh, J. Park, H. Lee, R. A. Langan, S. E. Boyken, M. J. Lajoie, L. Cao, C. M. Chow, M. C. Miranda, J. Wi, H. J. Hong, L. Stewart, B. H. Oh, D. Baker, De novo design of modular and tunable protein biosensors. *Nature* **591**, 482–487 (2021).
- F. Thomas, W. M. Dawson, E. J. M. Lang, A. J. Burton, G. J. Bartlett, G. G. Rhys, A. J. Mulholland, D. N. Woolfson, De novo-designed α -helical barrels as receptors for small molecules. *ACS Synth. Biol.* **7**, 1808–1816 (2018).
- P. J. Schnatz, J. M. Brisendine, C. C. Laing, B. H. Everson, C. A. French, P. M. Molinaro, R. L. Koder, Designing heterotropically activated allosteric conformational switches using supercharging. *Proc. Natl. Acad. Sci. U.S.A.* **117**, 5291–5297 (2020).
- D. H. Pike, V. Nanda, Empirical estimation of local dielectric constants: Toward atomistic design of collagen mimetic peptides. *Biopolymers* **104**, 360–370 (2015).
- G. S. Murphy, J. L. Mills, M. J. Miley, M. Machiusi, T. Szyperski, B. Kuhlman, Increasing sequence diversity with flexible backbone protein design: The complete redesign of a protein hydrophobic core. *Structure* **20**, 1086–1096 (2012).
- E. G. Emberly, N. S. Wingreen, C. Tang, Designability of alpha-helical proteins. *Proc. Natl. Acad. Sci. U.S.A.* **99**, 11163–11168 (2002).
- M. L. Peach, R. E. Cachau, M. C. Nicklaus, Conformational energy range of ligands in protein crystal structures: The difficult quest for accurate understanding. *J. Mol. Recognit.* **30**, e2618 (2017).
- V. Liegeois, *DrawMol* (University de Namur, 2018), vol. 1.4.30; www.unamur.be/drawmol.
- J. M. Wang, R. M. Wolf, J. W. Caldwell, P. A. Kollman, D. A. Case, Development and testing of a general amber force field. *J. Comput. Chem.* **25**, 1157–1174 (2004).
- C. B. Millard, G. Koellner, A. Ordentlich, A. Shafferman, I. Silman, J. L. Sussman, Reaction products of acetylcholinesterase and VX reveal a mobile histidine in the catalytic triad. *J. Am. Chem. Soc.* **121**, 9883–9884 (1999).
- D. L. Collins-Wildman, M. Kim, K. P. Sullivan, A. M. Plonka, A. I. Frenkel, D. G. Musaev, C. L. Hill, Buffer-induced acceleration and inhibition in polyoxometalate-catalyzed organophosphorus ester hydrolysis. *ACS Catal.* **8**, 7068–7076 (2018).
- A. White, Effect of pH on fluorescence of tyrosine, tryptophan and related compounds. *Biochem. J.* **71**, 217–220 (1959).
- National Research Council (US) Subcommittee on Guidelines for Military Field Drinking-Water Quality, *Guidelines for Chemical Warfare Agents in Military Field Drinking Water* (National Academies Press, 1995).
- G. Ortega, D. Mariottini, A. Troina, F. W. Dahlquist, F. Ricci, K. W. Plaxco, Rational design to control the trade-off between receptor affinity and cooperativity. *Proc. Natl. Acad. Sci. U.S.A.* **117**, 19136–19140 (2020).
- L. A. Lepak, P. Schnatz, I. Bendoy, D. Kosciolk, R. Koder, D. T. Crouse, Handheld chem/biosensor using extreme conformational changes in designed binding proteins to enhance surface plasmon resonance (SPR), in *Proceedings SPIE Advanced Environmental, Chemical, and Biological Sensing Technologies XII* (SPIE, 2016), vol. 9862.
- M. Kurnik, E. Z. Pang, K. W. Plaxco, An electrochemical biosensor architecture based on protein folding supports direct real-time measurements in whole blood. *Angew. Chem. Int. Ed.* **59**, 18442–18445 (2020).
- H. E. Pence, A. Williams, ChemSpider: An online chemical information resource. *J. Chem. Educ.* **87**, 1123–1124 (2010).
- D. A. Case, T. E. Cheatham, T. Darden, H. Gohlke, R. Luo, K. M. Merz, A. Onufriev, C. Simmerling, B. Wang, R. J. Woods, The Amber biomolecular simulation programs. *J. Comput. Chem.* **26**, 1668–1688 (2005).
- K. Vanommeslaeghe, E. P. Raman, A. D. MacKerell Jr., Automation of the CHARMM General Force Field (CGenFF) II: Assignment of bonded parameters and partial atomic charges. *J. Chem. Inf. Model.* **52**, 3155–3168 (2012).
- J. Wang, W. Wang, P. A. Kollman, D. A. Case, Automatic atom type and bond type perception in molecular mechanical calculations. *J. Mol. Graph.* **25**, 247–260 (2006).
- C. M. Summa, A. Lombardi, M. Lewis, V. F. DeGrado, Tertiary templates for the design of diiron proteins. *Curr. Opin. Struct. Biol.* **9**, 500–508 (1999).
- Y. P. Pang, FF12MC: A revised AMBER forcefield and new protein simulation protocol. *Proteins* **84**, 1490–1516 (2016).
- R. L. Dunbrack, M. Karplus, Backbone-dependent rotamer library for proteins—Application to side-chain prediction. *J. Mol. Biol.* **230**, 543–574 (1993).
- A. C. Mutter, J. A. Norman, M. T. Tiedemann, S. Singh, S. Sha, S. Morsi, I. Ahmed, M. J. Stillman, R. L. Koder, Rational design of a zinc phthalocyanine binding protein. *J. Struct. Biol.* **185**, 178–185 (2014).

Acknowledgments: We thank S. McPhee and R. Ulijn at the CUNY ASRC for the use of the infrared spectrophotometer. **Funding:** This work was supported in part by contracts FA4819-14-C-0017 and FA4819-C-17-0001 from the Air Force Civil Engineer Center, Tyndall AFB, FL. M.C.B. acknowledges support from the NIH (GM111932). **Author contributions:** J.J.M., D.H.P., M.C.B., D.T.C., V.N., and R.L.K. designed the research; J.J.M., D.H.P., M.C.B., and D.T.C. performed the research; J.J.M., D.H.P., V.N., and R.L.K. analyzed data; J.J.M., D.H.P., V.N., and R.L.K. wrote the paper. **Competing interests:** The authors declare that they have no competing interests. **Data and materials availability:** All data needed to evaluate the conclusions in the paper are present in the paper and/or the Supplementary Materials.

Submitted 2 March 2021

Accepted 20 May 2022

Published 6 July 2022

10.1126/sciadv.abh3421